

Hybridization kinetics is different inside cells

Ingmar Schoen, Hubert Krammer, and Dieter Braun¹

Systems Biophysics, Center for Nanoscience, Ludwig Maximilians Universität München, Amalienstraße 54, 80799 Munich, Germany

Edited by William A. Eaton, National Institutes of Health, Bethesda, MD, and approved October 21, 2009 (received for review February 10, 2009)

It is generally expected that the kinetics of reactions inside living cells differs from the situation in bulk solutions. Macromolecular crowding and specific binding interactions could change the diffusion properties and the availability of free molecules. Their impact on reaction kinetics in the relevant context of living cells is still elusive, mainly because the difficulty of capturing fast kinetics in vivo. This article shows spatially resolved measurements of DNA hybridization kinetics in single living cells. HeLa cells were transfected with a FRET-labeled dsDNA probe by lipofection. We characterized the hybridization reaction kinetics with a kinetic range of 10 μ s to 1 s by a combination of laser-driven temperature oscillations and stroboscopic fluorescence imaging. The time constant of the hybridization depended on DNA concentration within individual cells and between cells. A quantitative analysis of the concentration dependence revealed several-fold accelerated kinetics as compared with free solution for a 16-bp probe and decelerated kinetics for a 12-bp probe. We did not find significant effects of crowding agents on the hybridization kinetics in vitro. Our results suggest that the reaction rates in vivo are specifically modulated by binding interactions for the two probes, possibly triggered by their different lengths. In general, the presented imaging modality of temperature oscillation optical lock-in microscopy allows to probe biomolecular interactions in different cell compartments in living cells for systems biology.

DNA | in vivo | molecular crowding | temperature oscillation | optical lock-in microscopy

How does a cell react to a certain stimulus? Numerous biochemical reactions are orchestrated in both space and time to transmit and process information between different locations inside a single cell. In the past, studies of signaling networks focused on the identification of molecules, their binding partners, and different mechanisms of action. Such typically static investigations in vitro are increasingly complemented by imaging techniques in vivo (1–3) and computational systems biology methods to model the dynamic response on several levels (4–7). However, the necessary reaction rates are generally taken from measurements in vitro because of the lack of quantitative in vivo data (8). To fill this information gap, methods are needed to measure the reaction kinetics in its natural context, namely inside living cells.

Experimental knowledge about how reactions are influenced by the intracellular environment is sparse. On one hand, molecules are densely packed in the cellular space and could potentially act as barriers for diffusion or restrict molecular motion. These effects are subsumed under the loosely defined term molecular crowding (9, 10). It is expected that molecular crowding affects equilibrium properties and reaction kinetics and could impair the quantitative significance of existing models (8). Often, anomalous diffusion is taken as an indicator of molecular crowding (11, 12). But how it affects the kinetics of cellular reactions has not been addressed experimentally. However, selective interactions with reaction partners might significantly modulate kinetics in vivo as compared with the situation in vitro.

Here, we describe a method termed temperature oscillation optical lock-in (TOOL) microscopy for imaging reaction kinetics in living cells with optical resolution. It allows us to compare reaction kinetics in vivo with that in vitro. We apply the method

to measure hybridization of short dsDNA probes in HeLa cells and find clear indications for both accelerated and decelerated kinetics compared with identical solution measurements.

Principle of TOOL Microscopy

In general, ensemble measurements of reaction kinetics are performed by perturbing the system with an external stimulus and observing the relaxation behavior. The standard technique is to measure the response to a small temperature jump (13, 14). Here, we apply temperature oscillations instead of a jump (Fig. 1). At low oscillation frequencies, the concentrations of the reaction partners follow the stimulus instantaneously and oscillate with the temperature. At higher frequencies where the temperature oscillates faster than the reaction time constant, the concentrations oscillate with a phase delay and diminished amplitude. Both the delay time and the decreasing amplitude can be evaluated to obtain the reaction time constant. Mathematically, the exponential relaxation of the reaction translates to a transfer function in Fourier space that is used to fit the measurement data of a temperature oscillation protocol (see Eq. A1). The concept of oscillatory signals is widely used in electrical engineering and increasingly perceived as a useful tool to characterize biological networks and chemical reactions (15–20).

The TOOL approach requires a fluorescent readout of the reaction state (typically FRET) under external perturbation by small, laser-induced temperature oscillations (Fig. 1). The signal-to-noise ratio of fluorescence detection can be improved substantially by an optical lock-in scheme (21). Briefly, a frequency-locked stroboscopic illumination with four different delay times highlights certain phases of the reaction and allows retrieval of the amplitude and phase with a slow standard CCD camera (Fig. S1). This approach has been successfully used to image the conformational kinetics of a DNA hairpin (21). We adapted the method for the investigation of reaction kinetics in living cells (Fig. 1). Infrared laser light from below is absorbed by a chromium layer on a highly thermally conductive substrate, similar to previous approaches (22). HeLa cells can be seeded directly onto these object slides and kept in standard cell culture. Temperature oscillations with an amplitude of ≈ 2.5 K and a relaxation time constant of ≈ 200 μ s are applied with a defocused infrared laser as measured with temperature-sensitive fluorescence (see *SI Text*).

Results

Monitoring DNA Hybridization with FRET. The hybridization of two complementary and antiparallel strands of nucleic acids is a specific example for a reversible bimolecular reaction. We monitored the opening and closing of 12- and 16-bp dsDNA probes with an internal FRET pair (23) of rhodamine green

Author contributions: I.S. and D.B. designed research; I.S. and H.K. performed research; I.S. and D.B. analyzed data; and I.S., H.K., and D.B. wrote the paper.

The authors declare no conflict of interest.

This article is a PNAS Direct Submission.

Freely available online through the PNAS open access option.

¹To whom correspondence should be addressed. E-mail: dieter.braun@physik.uni-muenchen.de.

This article contains supporting information online at www.pnas.org/cgi/content/full/0901313106/DCSupplemental.

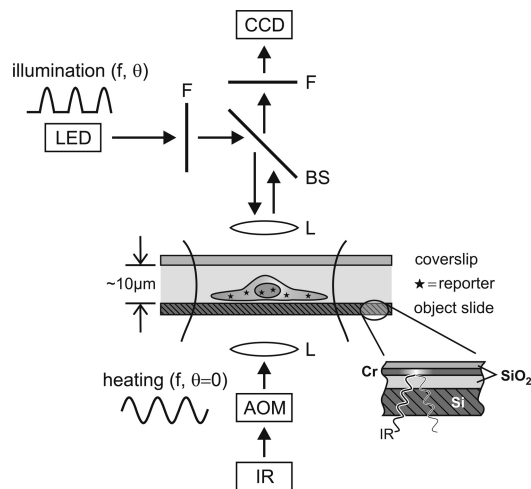


Fig. 1. TOOL microscopy. An IR laser (wavelength 1,455 nm) is heating the bottom of a cell culture chamber. Fast heat retraction is accomplished by a silicon substrate and thin chamber dimensions. Both heating and illumination are modulated with a tunable phase shift θ and imaged with a standard CCD camera. AOM, acousto-optical modulator; L, lens; LED, light-emitting diode; F, filter; BS, beam splitter.

(RhG) and carboxyl-X-rhodamine (ROX). (Fig. 2*A*). Spacing at a distance of seven bases and short linkers avoided contact quenching (24). A BLAST search was performed with the sequence of the 16-mer to minimize specific interactions with genomic DNA or messenger RNA. Each strand was capped at both ends by an enantiomeric cytosine (L-nucleotide) (25) to suppress degradation by exonucleases (26). Lipofection was used for DNA delivery into the cells (26).

Excitation of the donor resulted in two emission peaks at 530 and 610 nm (Fig. S5*A*). With increasing temperature, donor fluorescence increased and FRET diminished; both yielding sigmoidal melting curves with a melting temperature of 31 °C (12-mer) and 35 °C (16-mer). As seen in Fig. 2*B*, temperature changes between 25 °C and 30 °C give rise to detectable fluorescence changes (gray underlay). The fact that the anticorrelated donor and FRET signals provide two separate measures for the same hybridization reaction is a good control for the origin of the signal.

The exogenous DNA probe was transferred into HeLa cells by lipofection and confocal images were taken to visualize its dissemination inside the cell (Fig. S5*B*). Both strands were evenly distributed over the cytoplasm and showed an enhanced concentration inside the nucleus (26). An overlay of donor and acceptor images showed that the two strands colocalized. The detection of FRET demonstrated the presence of duplexes throughout the cell and the stability of the labeled strands against degradation.

Imaging of the Reaction Kinetics. We applied periodic heating between 1 and 200 Hz to a cell transfected with the 16-mer and measured the donor and FRET signals by the described lock-in method. Both signals were then corrected against the temperature reference recorded in the vicinity of the cell (Fig. S4). The donor signal (Fig. 2*C*) described a lower half-circle in the complex plane that corresponds to a positive amplitude signal as expected from the positive slope of the RhG melting curve (see Fig. 2*B*). The transition occurred at a time constant of ≈ 35 ms. At high frequency, the signal settled around $-0.8\%/K$ that represents the intrinsic temperature sensitivity of the RhG dye. The FRET signal (Fig. 2*D*) shows negative amplitude in accordance with the negative slope of the FRET melting curve. The

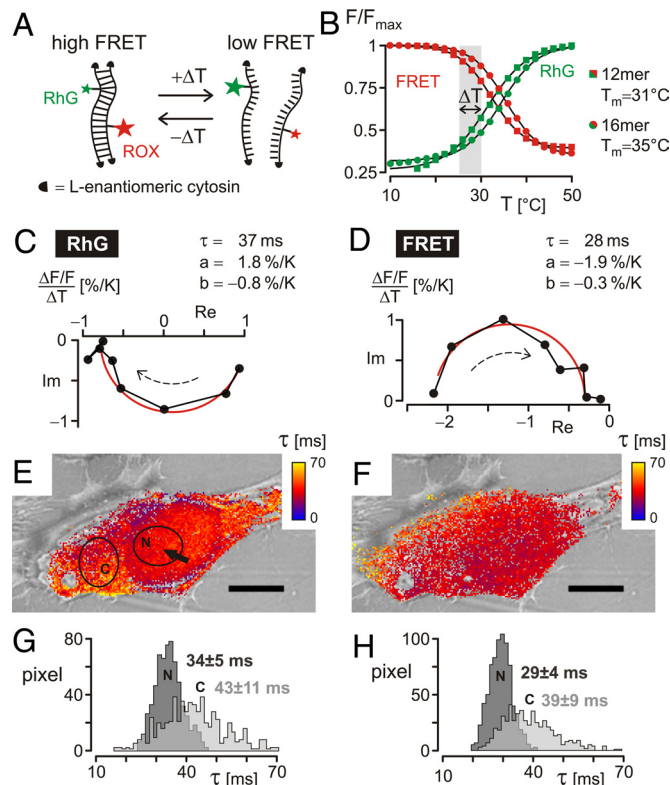


Fig. 2. Hybridization kinetics inside a single HeLa cell. (A and B) dsDNA probe design: (A) Complementary strands were labeled with the FRET pair RhG (donor) and ROX (acceptor) and left-handed chimeric cytosines at 3' and 5' ends to suppress degradation. Melting curves for the donor (green) and the FRET (red) signals were anticorrelated and fitted by melting temperatures of ≈ 31 °C for the 12-mer (squares) and ≈ 35 °C for the 16-mer (circles), respectively. (C and D) Transfer function and best fit (red line) at frequencies 1–200 Hz for a single pixel (arrow in *E*) for the 16-bp probe. The reaction amplitudes of the donor (C) and the FRET signal (D) show equal magnitude but opposite signs. (E and F) Cellular maps of the hybridization time constant show highly similar kinetics in both the donor and the FRET channel. (Scale bars: 10 μm .) (G and H) Histograms from nuclear (N) and cytoplasmic (C) regions (ellipses in *E*). Within the error bars, donor and FRET signals yielded identical results. Values are mean \pm SD.

fitted time constant of 28 ms was similar to that derived from the RhG measurement. The residual temperature sensitivity of $-0.3\%/K$ is expected from the mixed sensitivities of ROX and RhG in the FRET channel. The good agreement of the fitted characteristic temperature sensitivities and the anticorrelation of the donor and FRET signals verify their origin in the hybridization reaction.

We reconstructed a cellular map of the reaction time constant for the donor and the FRET signal (Fig. 2*E* and *F*). For both, the time constant varied between 20 and 70 ms depending on the location inside the cell. The kinetics were significantly faster inside the nucleus as compared with the rest of the cell as shown by histograms over representative regions (Fig. 2*G* and *H*). Donor and FRET signals revealed an average time constant of 30 ms in the nucleus as compared with 40 ms in the cytoplasm.

We performed kinetic measurements with the 16-bp DNA probe for 16 individual cells and with the 12-bp DNA probe for 10 cells. Three examples of each are shown in Fig. 3*A* and *B*, respectively. In all cases, the kinetics in the nucleus is distinctly faster than in the cytoplasm (see Fig. 3, histograms). In some cases, imaging resolved differences between nucleoli and the rest of the nucleus with slower kinetics in the nucleoli (Fig. S6), demonstrating kinetic imaging contrast of subcellular features.

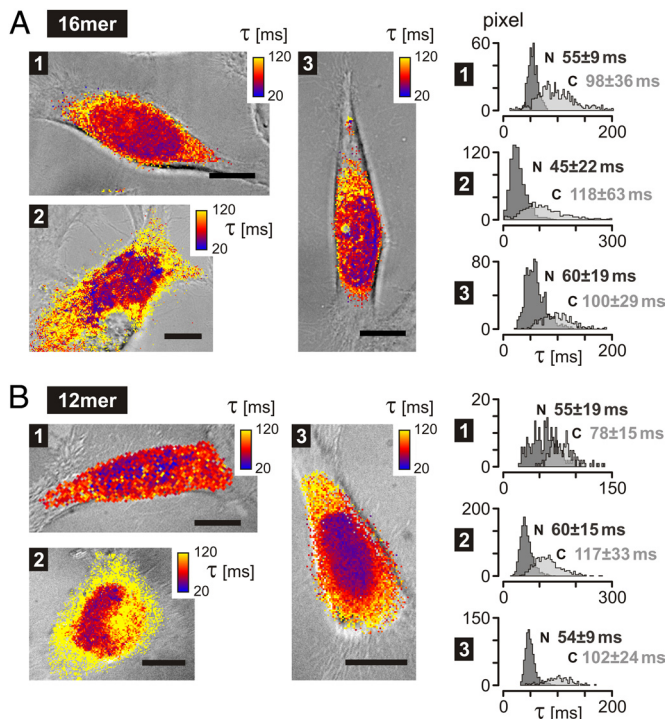


Fig. 3. Reaction speed in cellular compartments. (A) Shown is the 16-bp DNA probe. Maps of the reaction time constant (color-coded) for three individual cells and respective histograms from nuclear (N) and cytoplasmic (C) regions are shown. (B) As in A for a 12-bp DNA probe. Hybridization kinetics were always faster in the nucleus. (Scale bars: 10 μm .)

Concentration Dependence. Where do the above differences in the time constant arise from? One important parameter that influences the reaction speed of a second-order reaction is the concentration of reactants. If we neglect side reactions of the probe for now, we expect a time constant of the form $\tau^{-1} = k_{\text{off}} + k_{\text{on}} ([D] + [A])$ (27) where the off rate k_{off} represents the dissociation of the duplex and its formation is determined by free donor and acceptor concentrations ($[D]$, $[A]$) and an on rate k_{on} . For a 1:1 mixture ($[D] = [A]$), and with the total DNA concentration $c_{\text{DNA}} = [A] + [DA]$ we obtain

$$\tau^{-1} = \sqrt{k_{\text{off}}(k_{\text{off}} + 4k_{\text{on}}c_{\text{DNA}})} \quad [1]$$

(see *Materials and Methods*). A plot of the inverse time constant versus the DNA concentration thus yields a horizontal half-parabola whose intercept with the τ^{-1} axis is given by the off rate and whose slope is determined by the on rate.

Confocal images of the acceptor brightness were used to measure the DNA concentration. As calibration, we determined the brightness of the DNA probe in solutions of known concentration (Fig. S7A). We correlated the hybridization kinetics in the nuclei or cytosolic regions of single cells with their respective DNA concentration. The data of ≈ 10 individual cells are plotted for the 16-mer in Fig. 4A and for the 12-mer in Fig. 4C. The reverse time constant increased with increasing concentration in agreement with Eq. 1. On average, the data from the cytosole and nuclear regions followed the same trend, except for a few outliers for the cytosole.

For comparison, we measured the hybridization kinetics in free buffer solution. The in vitro data (Fig. 4B and D) again followed a marked concentration dependence (Eq. 1). Comparing the inverse time constant for the two probes, we found three times faster kinetics for the 12-mer compared with the 16-mer, as is expected from its shorter length. Surprisingly, a comparison

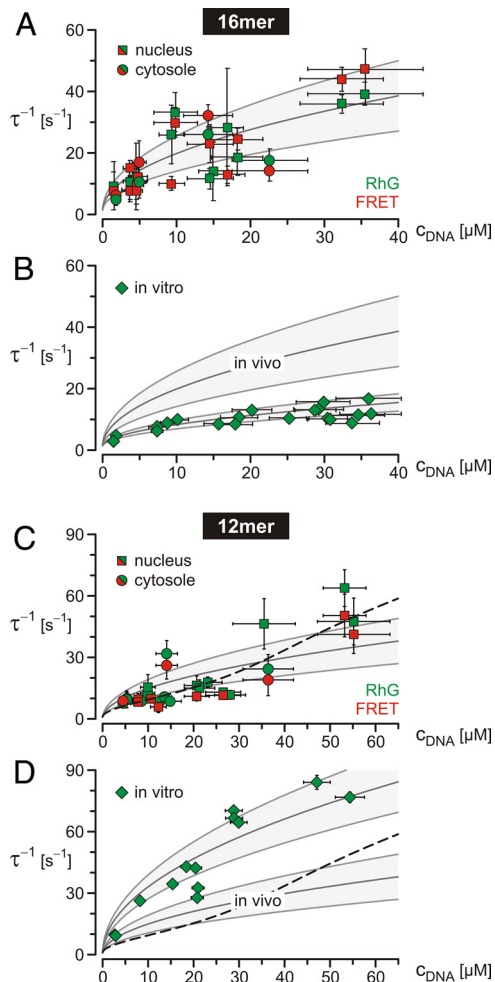


Fig. 4. Different kinetics in vivo compared with in vitro for the 16-bp DNA (A and B) and the 12-bp DNA (C and D). The inverse time constant τ^{-1} is plotted versus dsDNA concentration. Data are given as mean \pm SD together with the best fit of Eq. 1 (solid line) and its 95% confidence interval (gray). In vivo experiments comprise data from nuclear and cytosolic regions of >10 individual cells. They overlapped and were treated as a single dataset during fitting. The in vivo data of the 16-mer (A) were well described by the parabolic fit, whereas the shape of the 12-mer data (C) was better described by a buffered kinetics (dashed line; see *SI Text*). As compared with in vivo, the experiments in vitro showed slower kinetics of the 16-bp DNA (B) whereas the kinetics of 12-bp DNA (D) was distinctly faster.

with the in vivo measurements revealed a completely different behavior for the two probes: whereas the kinetics of the 16-mer was distinctly faster within cells, the kinetics of the 12-mer was slowed down in vivo.

Reaction Rates. We fitted the data by Eq. 1 to elucidate the changes in the underlying reaction rates. For the 16-mer, we obtained an on rate of $2.9 \times 10^7 \text{ M}^{-1}\text{s}^{-1}$ in vivo that was 7-fold larger than $4.2 \times 10^6 \text{ M}^{-1}\text{s}^{-1}$ in vitro (Fig. 4A and B, solid lines). In a distinct contrast, we obtain for the 12-mer an on rate of $5.5 \times 10^6 \text{ M}^{-1}\text{s}^{-1}$ in vivo that was ≈ 5 -fold smaller than the on rate of $2.7 \times 10^7 \text{ M}^{-1}\text{s}^{-1}$ in vitro. In contrast to the in vitro data, the in vivo data of the 12-mer were not well described by the parabolic relation but rather tended to be smaller at small concentrations and larger at high concentrations. We will describe this deviation later. Because of the lack of data at very low concentrations, the off rate was ill-defined and thus held constant during fitting. The above results were independent of the

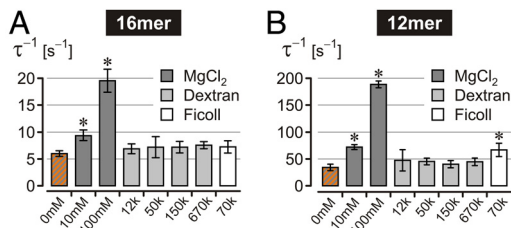


Fig. 5. Effect of divalent ions and crowding agents on the hybridization kinetics in vitro for the 16-bp probe (A) or the 12-bp probe (B). Magnesium chloride speeded up the reaction, whereas dextrans and Ficoll had only a minor impact on the kinetics. DNA concentration was 20 μ M; crowding agents had a final concentration of 20% (wt/vol). Error bars represent the SEM of four independent experiments. Asterisks indicate a significant difference between the sample against the reference in pure PBS (orange) according to Student's *t* test to the level $P < 0.01$.

choice of off rates that could be equally well fitted within a range from 0.1 to 4 s^{-1} . In accordance with the melting curve in vitro and literature data (28) we fixed the off rate to 0.3 s^{-1} for the 16-mer and 1.0 s^{-1} for the 12-mer.

Kinetics with Crowding Agents. To probe the effects of molecular crowding and divalent ions, we measured both DNA probes in vitro under various buffer conditions (Fig. 5). We found a significant acceleration in the reaction kinetics for Mg^{2+} . Interestingly, crowding agents barely affected the hybridization kinetics. At a concentration of 20% (wt/vol) that approaches the situation in vivo (9), highly branched dextrans of various molecular mass or the globular molecule Ficoll-70 barely enhanced the kinetics, with the only significant difference in the case of the 12-mer. A deceleration of the hybridization kinetics was never observed for any of the tested conditions and probes.

Discussion

Unspecific Modulation of Hybridization Kinetics. The measured hybridization rates in vitro for the 16-mer and the 12-mer dsDNA (Fig. 5) agree well with literature data from other solution measurements (29–31). However, the in vivo findings for the two dsDNA probes are surprising because the kinetics of the 16-mer was substantially speeded up, whereas that of the 12-mer was considerably slowed down. As we will discuss below, this finding is hardly explained without the aid of introducing DNA binding partners.

Macromolecular crowding is considered to change reaction kinetics in two ways: on one hand, an excluded volume predicts accelerated kinetics as a result from an enhanced effective concentration (10). Estimates of the excluded volume in the cytoplasm range from 20% to 30% (9), thereby increasing the effective probe concentration and thus the on rate by a factor of 1.2–1.4. In the nucleus, crowding effects might be even more pronounced. For example, a complex nucleoprotein network confines DNA and accelerates DNA repair by homologous search (46). However, macromolecular crowding leads to hindered diffusion (9) and potentially slows down reaction kinetics. A power-law dependence of the diffusion coefficient inside the nucleus (11, 12) supports these ideas. However, our experiments neither showed significant kinetic differences between the cytosole and the nucleus (Fig. 4 A and C), nor between in vitro measurements with or without crowding agents (Fig. 5). Molecular crowding apparently has only a minor impact on the hybridization kinetics of short DNA strands.

We do not expect variations in the calibration of DNA concentration. An underestimation of the fluorescence-measured concentration of oligonucleotides in cells could be wrongly attributed to an enhanced on rate. For example, the

concentration calibration can be misguided through intracellular fluorescence quenching by reducing agents (32) or bleaching. However, control measurements with glutathione and ascorbic acid at typical intracellular concentrations (33, 34) showed only an effect of a few percent on the determined concentration (Fig. S7B). The effect of bleaching was also small as evaluated from images taken at the beginning and the end of a cell measurement.

Hydrophobic or electrostatic interactions might differentially affect the stability of either the ssDNA, the duplex, or intermediate structures (10). For example, a differentially reduced electrostatic repulsion of ssDNA enhances the association rate of hybridization (35). Divalent ions show this effect as confirmed by in vitro measurements demonstrating a strong acceleration with increasing $MgCl_2$ concentration for both probes (Fig. 5). But even if cells do implement such considerably enhanced ionic shielding to explain the 7-fold enhanced on rate of the 16-mer, the conditions equally would affect the 12-mer.

Probe-Specific Modulation of Hybridization Kinetics. The mechanisms discussed so far cannot explain why the hybridization kinetics of the 12-bp probe was differentially modulated as compared with the 16-bp probe inside cells. In the following we discuss examples of binding partners that have the potential to distinguish between the two probes and eventually describe the differentially modified kinetics (Fig. 4 A and C).

Interference RNA, messenger RNA or freely available genomic sequences are probably able to interact with the probe dynamically and in a length-dependent manner. A randomized sequence space for these endogenous oligonucleotides would yield $4 \times 4^4 \approx 1,000$ times more abundant binding sites for the 12-mer as compared with the 16-mer. If this background binding shows similar on and off rates as the probe reaction, it enhances the reaction speed by adding with its concentration c_B to the probe concentration c_{DNA} in Eq. 1. The plot of the reaction speed shifts to the left and primarily enhances the kinetics for small probe concentrations (see Fig. S8). The in vivo data did not show such an offset nor was the 12-mer stronger accelerated than the 16-mer; in fact, we observed quite the opposite. Both findings make the above scenario improbable.

Proteins in the cell can interact specific and unspecific with ssDNA and dsDNA and can thereby either speed up or slow down the reaction, depending on the type of interaction. We distinguish two cases:

Recombination mediator proteins, as for example Rad52, catalyze and thereby accelerate the hybridization of complementary ssDNA in the context of homologous recombination, DNA repair, and rescue of collapsed replication forks. Thousandfold accelerated annealing rates have been reported for Rad52 (36, 37). The annealing efficiency has been shown to be higher toward longer DNA strands, although no oligos shorter than 15 bp were investigated (38). This finding might hint toward a selective acceleration of the 16-mer in the nucleus; however, it remains unclear whether such a mechanism also exists in the cytosole as found in our measurements. In the simplest model, we account for these effects by enhancing the on rate in Eq. 1 as we did in the fit for the 16-mer (Fig. 4A, solid line).

Other DNA-binding proteins can stabilize ssDNA or dsDNA and thus slow down the annealing kinetics by reducing the concentration of free reactants. An example for a ssDNA-binding (SSB) protein is replication protein A (39), whereas HMG-motif proteins (40) are prototypical dsDNA-binding (DSB) proteins. Both usually tend to bind stronger to longer constructs (39, 40), and some evidence exists that they also reside in the cytosole (39). A stabilization of the DNA strands requires slower binding kinetics as compared with the probe reaction and renders the background binding quasi-stationary. We modeled the binding to either ssDNA or dsDNA with an equilibrium constant K_B and a binder concentration c_B as derived in *SI Text*.

The previously not described deceleration of the 12-mer compared with its *in vitro* kinetics can be convincingly fitted by either DSB interactions with $c_B = 36 \mu\text{M}$ and $K_B = 5.4 \cdot 10^5$ (Fig. 4C, dashed line) or SSB interactions with $c_B = 135 \mu\text{M}$ and $K_B = 6.1 \cdot 10^5$ (see Fig. S9C). Notably, both fits described the shape of the data better than the parabolic Eq. 1.

Thus, the modulation of hybridization kinetics *in vivo* is likely the result of two opposite effects. On the one hand, recombination mediator proteins or divalent ions can describe the 7-fold increase of the association rate for the 16-mer in its magnitude. However, buffering of probe strands by e.g., DSB proteins can explain the slowed kinetics of the 12-mer. We implicitly assumed that the acceleration was specific for the 16-mer and the buffering only affected the 12-mer. However, both effects might act stronger, but in concert: our data are consistent with a 16-mer with strong enhancement of the association rate under minor buffering and a 12-mer with slight enhancement of the association rate and strong buffering (Fig. S9). This means that the 7-fold acceleration of the on rate and the 5-fold deceleration caused by buffering are lower bounds to the actual *in vivo* changes. Overall, *in vivo* imaging of DNA reaction kinetics in living cells indicates that hybridization kinetics is under significant differential control. In our case, factors of molecular crowding appear to be of limited importance.

TOOL Microscopy. The advantages of using the frequency space approach of TOOL compared with conventional temperature jump and time-lapse imaging are manifold: the kinetic range is not restricted by the camera speed, the method is compatible with standard fluorescence microscopy and thus applicable to cells, the signal-to-noise ratio is significantly enhanced by the lock-in approach, and neither the intrinsic temperature sensitivity of the dye nor bleaching hamper the relaxation analysis. As an established alternative, kinetics can be measured by fluorescence correlation spectroscopy (FCS) under true equilibrium conditions even in living cells (11, 12), yet with some restrictions. The short residence time of molecules in the focus restricts FCS to fast, typically intramolecular kinetics. Low concentrations are required to record an autocorrelation signal. Several extensions of the FCS principle have the potential to overcome these limitations in the future (41, 42). To date, TOOL microscopy is a useful complement of FCS-based techniques, because it works at high concentrations, has a kinetic range distinct from FCS, and provides fast and comparably simple direct imaging.

The requirements of TOOL microscopy with respect to the probe are very general: the readout can be any fluorescence property and the nature of the probe itself is of minor importance. For example, binding of small labeled DNA or RNA molecules to larger proteins could be visualized by changes in their fluorescence anisotropy. Protein-protein interactions could be monitored by FRET between two fluorescent proteins or two organic dyes fused to genetic tags (43). This will enable the comprehensive investigation of reactions in signaling networks. The kinetic range reaches from $\approx 10 \mu\text{s}$ to 1 s and is restricted on the one side by the retrieval of the phase at high frequencies and on the other side by long measurement times for very slow oscillations. TOOL will help to establish *in vivo* test systems for computational modeling and will be used to probe effects of molecular crowding in cellular compartments.

Outlook

To conclude, we developed TOOL microscopy to image kinetics at the tens of microsecond to second scale inside living cells. We measured the kinetics of DNA hybridization in the cytosol and the nucleus and found an unexpected strong, probe-dependent modification compared with *in vitro* measurements. The application of TOOL microscopy to protein-protein reactions is anticipated.

Materials and Methods

Lock-In Imaging. An upright microscope (Axiotech Vario; Zeiss) was equipped with a 100 \times oil-immersion objective (CFI Apochromat TIRF; Nikon). The beam of a fiber-coupled near-infrared laser (RLD-5-1455; IPG Laser) was modulated by an acousto-optical modulator (AA.DTS.XY.100; Pegasus Optik) and weakly focused (C240TM-C; Thorlabs) to a FWHM of 150 μm in the chamber. Illumination was provided by cyan or red light-emitting diodes (Luxeon III Star; Philips). A CCD camera (SensiCam QE; PCO) imaged with 1-s exposure time and 2×2 or 4×4 binning was used.

Signals were generated by two synchronized A/D cards (PCI-6229 and PCI-6221; National Instruments) under LabView control. The IR laser intensity followed $I_{IR} = 0.5\Delta I_{IR}[\sin(2\pi f \cdot t) + 1]$ with a maximum power $\Delta I_{IR} = 2.5 \text{ W}$. Illumination patterns were composed of upper halves of a sine wave $I_{LED} = \Delta I_{LED}\Theta[\sin(2\pi f t - \theta)]\sin(2\pi f t - \theta)$ with a phase lag θ (21). To correct for bleaching, images were taken in the order $\theta = 0^\circ|180^\circ|270^\circ|90^\circ|B|B|90^\circ|270^\circ|180^\circ|0^\circ$ (B = without illumination). Intracellular hybridization kinetics (Figs. 2–4) was investigated for $f = 1 \dots 200 \text{ Hz}$. The temperature reference was recorded by lateral translation of the sample and recording Cy5 fluorescence next to the cell. Intracellular temperature kinetics (Fig. S2) was recorded for $f = 20 \dots 1,000 \text{ Hz}$. Cell viability was routinely checked before and after the experiment (Fig. S3).

As a side note, the herein described optical lock-in (21) has to be distinguished from a more recent method with a similar name (44, 45) that uses filtering in Fourier space to remove nonperiodic contributions from a reversibly switched fluorescence signal.

Data Analysis. The complex transfer function $h(f)$ of the fluorescence response was reconstructed from the image series for each frequency by summation of image pairs at identical phases and applying

$$h(f) = \frac{4}{\pi} \left[\frac{I_{0^\circ} - I_{180^\circ}}{I_{0^\circ} + I_{180^\circ} - 2I_{back}} + i \frac{I_{270^\circ} - I_{90^\circ}}{I_{270^\circ} + I_{90^\circ} - 2I_{back}} \right] \quad [\text{A1}]$$

(21). For temperature measurements, fluorescence amplitudes were translated to temperature changes via the Cy5 calibration. The RhG or FRET transfer function was divided by the respective temperature transfer function for each frequency (see Fig. S5). The resulting hybridization transfer function was fitted pixelwise by Eq. 1. Artifacts from overexposed pixels were removed and poor fits were filtered out by a threshold to the mean square error. The amplitude was corrected against background fluorescence by taking the mean fluorescence intensity I_{back} in the vicinity of the cell and rescaling the fitted amplitude by $I/(I - I_{back})$, with I being the fluorescence intensity at the respective image pixel.

Transfer Function of Reaction. The temporal relaxation of the fluorescence signal after a small temperature jump adopts a single exponential time course $\Delta F(t) = a \exp(-t/\tau) + b \cdot \Theta(t)$ with a characteristic time constant τ , an amplitude a that depicts the concentration change for $t \rightarrow \infty$, and an instantaneous offset b caused by the intrinsic temperature sensitivity of the dye. The corresponding response in the frequency domain is derived from this formula by a Laplace transformation. It is given by the transfer function $h(f)$ that assigns a complex valued concentration response to a certain stimulation frequency f . The mono-exponential relaxation kinetics transforms to

$$h(f) = \frac{a}{1 + i \cdot 2\pi f \cdot \tau} + b \quad [\text{A2}]$$

with a , b , and τ as above (21). A plot of $h(f)$ in the complex plane illustrates the characteristic transition (Fig. S1).

Determination of Local DNA Concentration. A multipoint confocal scanner (vlnfinity2; Visitron Systems) with an EMCCD camera (Cascade II; Photometrics) was mounted to a second output of the microscope. The illumination with either 488 or 561 nm was restricted to 5 mW to minimize bleaching. Laser intensity, scanning parameters, filters, and camera settings were identical for all confocal images, the only variable parameter was the exposure time. The fluorescence intensity of ROX was determined confocally, weighted with the exposure time, and calibrated against identically prepared chambers containing dsDNA concentrations of 3.6, 8, 16, 22, 28, and 36 μM in PBS buffer (see Fig. S7). Slides were pretreated by a plasma cleaning to prevent adsorption of DNA.

Concentration Dependence of the Time Constant. The relaxation time constant

of the reaction $A + D \xrightleftharpoons[k_{off}]{k_{on}} AD$ is given by $\tau^{-1} = k_{off} + k_{on}([D] + [A])$ (27).

Starting from the equilibrium condition $k_{off}[DA] = k_{on}[D][A]$ we set $[D] = [A]$ for the used 1:1 mixture, added $k_{off}[A]$ on both sides, and obtained $k_{off}([A] + [DA]) = k_{on}[A]^2 + k_{off}[A]$. We defined $c_{DNA} = [A] + [DA]$, replaced the bracketed term on the left side, solved for $[A]$, and found $[A] = (k_{off} + \sqrt{k_{off}^2 + 4k_{on}k_{off}c_{DNA}})/(2k_{on})$. Inserting this into the above relation for the time constant yielded Eq. 1.

- Lippincott-Schwartz J, Snapp E, Kenworthy A (2001) Studying protein dynamics in living cells. *Nat Rev Mol Cell Biol* 2:444–456.
- Miyawaki A (2003) Visualization of the spatial and temporal dynamics of intracellular signaling. *Dev Cell* 4:295–305.
- Giepmans BNG, Adams SR, Ellisman MH, Tsien RY (2006) The fluorescent toolbox for assessing protein location and function. *Science* 312:217–224.
- Ideker T, Galitski T, Hood L (2001) A new approach to decoding life: Systems biology. *Annu Rev Genomics Hum Genet* 2:343–372.
- Di Ventura B, Lemerle C, Michalodimitrakis K, Serrano L (2006) From in vivo to in silico biology and back. *Nature* 443:527–533.
- Fisher J, Henzinger TA (2007) Executable cell biology. *Nat Biotechnol* 25:1239–1249.
- Zhang S, Jin G, Zhang XS, Chen L (2007) Discovering functions and revealing mechanisms at molecular level from biological networks. *Proteomics* 7:2856–2869.
- Takahashi K, Arjunan SNV, Tomita M (2005) Space in systems biology of signaling pathways: Toward intracellular molecular crowding in silico. *FEBS Lett* 579:1783–1788.
- Ellis RJ (2001) Macromolecular crowding: Obvious but underappreciated. *Trends Biochem Sci* 26:597–604.
- Minton AP (2006) How can biochemical reactions within cells differ from those in test tubes? *J Cell Sci* 119:2863–2869.
- Weiss M, Elsner M, Kartberg F, Nilsson T (2004) Anomalous subdiffusion is a measure for cytoplasmic crowding in living cells. *Biophys J* 87:3518–3524.
- Guigas G, Kalla C, Weiss M (2007) The degree of macromolecular crowding in the cytoplasm and nucleoplasm of mammalian cells is conserved. *FEBS Lett* 581:5094–5098.
- Eigen M (1954) Methods for investigation of ionic reactions in aqueous solutions with half-times as short as 10^{-9} sec. *Faraday Discuss* 17:194–205.
- Kirschner K, Eigen M, Bittman R, Voigt B (1966) The binding of nicotinamide-adenine dinucleotide to yeast D-glyceraldehyde-3-phosphate dehydrogenase: Temperature-jump relaxation studies on the mechanism of an allosteric enzyme. *Proc Natl Acad Sci USA* 56:1661–1667.
- Pörschke D, Nolte G (1994) Deconvolution of electrooptical data in the frequency domain: Relaxation processes of DNA from rigid rods to coiled spheres. *Macromology* 27:590–595.
- Lipan O, Wang WH (2005) The use of oscillatory signals in the study of genetic networks. *Proc Natl Acad Sci USA* 102:7063–7068.
- Berthoumieux H, Jullien L, Lemarchand A (2007) Response to a temperature modulation as a signature of chemical mechanisms. *Phys Rev E* 76:056112.
- Bennet MR, et al. (2008) Metabolic gene regulation in a dynamically changing environment. *Nature* 454:1119–1122.
- Ingolia NT, Weissman JS (2008) Reverse engineering the cell. *Nature* 454:1059–1061.
- Mettetal JT, Muzzey D, Gómez-Urbe C, van Ourdenaarden A (2008) The use of oscillatory signals in the study of genetic networks. *Science* 319:482–484.
- Braun D, Libchaber A (2003) Lock-in by molecular multiplication. *Appl Phys Lett* 83:5554–5556.
- Zondervan R, et al. (2006) Laser-driven microsecond temperature cycles analyzed by fluorescence polarization microscopy. *Biophys J* 90:2958–2969.
- Cardullo RA, et al. (1988) Detection of nucleic acid hybridization by nonradiative fluorescence resonance energy transfer. *Proc Natl Acad Sci USA* 85:8790–8794.
- Marras SAE, Kramer FR, Tyagi S (2002) Efficiencies of fluorescence resonance energy transfer and contact-mediated quenching in oligonucleotide probes. *Nucleic Acids Res* 30:e122.
- Damha MJ, Giannaris PA, Marfey P (1994) Antisense L/D-oligodeoxynucleotide chimeras: Nuclease stability, base-pairing properties, and activity at directing ribonuclease H. *Biochemistry* 33:7877–7885.
- Sixou S, et al. (1994) Intracellular oligonucleotide hybridization detected by fluorescence resonance energy transfer (FRET). *Nucleic Acids Res* 22:662–668.
- Mortimer RG (2008) *Physical Chemistry* (Elsevier Academic, London).
- Ikuta S, Takagi K, Wallace R, Itakura K (1987) Dissociation kinetics of 19 base-paired oligonucleotide-DNA duplexes containing different single mismatched base pairs. *Nucleic Acids Res* 15:797–811.
- Parkhurst KM, Parkhurst LJ (1995) Kinetic studies by fluorescence resonance energy transfer employing a double-labeled oligonucleotide: Hybridization to the oligonucleotide complement and to single-stranded DNA. *Biochem* 34:285–292.
- Sekar MMA, Bloch W, St John PM (2005) Comparative study of sequence-dependent hybridization kinetics in solution and on microspheres. *Nucleic Acids Res* 33:366–375.
- Gao Y, Wolf LK, Geordiadis RM (2006) Secondary structure effects on DNA hybridization kinetics: A solution versus surface comparison. *Nucleic Acids Res* 34:3370–3377.
- Lakowicz JR (1999) *Principles of Fluorescence Spectroscopy* (Kluwer Academic, New York).
- Winkler BS, Orsellini SM, Rex TS (1994) The redox couple between glutathione and ascorbic acid: A chemical and physiological perspective. *Free Radical Biol Med* 17:333–349.
- Valko M, et al. (2006) Free radicals, metals, and antioxidants in oxidative stress-induced cancer. *Chem Biol Interact* 160:1–40.
- Williams AP, Longfellow CE, Freier SM, Kierzek R, Turner DH (1989) Laser temperature jump, spectroscopic, and thermodynamic study of salt effects on duplex formation by dGCATGC. *Biochemistry* 28:4283–4291.
- Mortensen UH, Bendixen C, Sunjevaric I, Rothstein R (1996) DNA strand annealing is promoted by the yeast Rad52 protein. *Proc Natl Acad Sci USA* 93:10729–10734.
- Sugiyama T, New JH, Kowalczykowski SC (1998) DNA annealing by Rad52 Protein is stimulated by specific interaction with the complex of replication protein A and single-stranded DNA. *Proc Natl Acad Sci USA* 95:6049–6054.
- Rothenberg E, et al. (2008) Human Rad52-mediated homology search and annealing occurs by continuous interactions between overlapping nucleoprotein complexes. *Proc Natl Acad Sci USA* 105:20274–20279.
- Wold MS (1997) Replication protein A: A heterotrimeric, single-stranded DNA-binding protein required for eukaryotic DNA metabolism. *Annu Rev Biochem* 66:61–92.
- Bustin M (1999) Regulation of DNA-dependent activities by the functional motifs of the high-mobility-group chromosomal proteins. *Mol Cell Biol* 19:5237–5246.
- Burkhardt M, Schwille P (2006) Electron multiplying CCD based detection for spatially resolved fluorescence correlation spectroscopy. *Opt Expr* 14:5013–5020.
- Ries J, Schwille P (2006) Studying slow membrane dynamics with continuous wave scanning fluorescence correlation spectroscopy. *Biophys J* 91:1915–1924.
- O'Hare HM, Johnson K, Gautier A (2007) Chemical probes shed light on protein function. *Curr Opin Struct Biol* 17:488–494.
- Mao S, et al. (2008) Optical lock-in detection of FRET using synthetic and genetically encoded optical switches. *Biophys J* 94:4515–4524.
- Marriott G, et al. (2008) Optical lock-in detection imaging microscopy for contrast-enhanced imaging in living cells. *Proc Natl Acad Sci USA* 105:17789–17794.
- Minsky A (2003) Strural aspects of DNA repair: The role of restricted diffusion. *Mol Microbiol* 50:367–376.